Astron. Astrophys. 354, 1021–1035 (2000)

ASTRONOMY AND ASTROPHYSICS

The corona of the dMe flare star AD Leo

F. Favata[1], **G. Micela**[2], **and F. Reale**[3]

[1] Astrophysics Division – Space Science Department of ESA, ESTEC, Postbus 299, 2200 AG Noordwijk, The Netherlands
[2] Osservatorio Astronomico di Palermo, Piazza del Parlamento 1, 90134 Palermo, Italy
[3] Univ. Palermo, Dip. Scienze FF. & AA., Sez. Astronomia, Piazza del Parlamento 1, 90134 Palermo, Italy

Received 24 August 1999 / Accepted 29 November 1999

Abstract. We have systematically studied the X-ray emission (both the quiescent component and the flares) of the dM3e star AD Leo, analyzing the existing observations from the *Einstein* IPC, ROSAT PSPC and ASCA SIS instruments. Using a consistent method which explicitly considers the possibility of sustained heating we have analyzed the six flares which have sufficient statistics, deriving constraints on the physical parameters of the flaring regions. In all cases the flaring loops are likely compact ($L \simeq 0.3\ R_*$), and confined to a rather narrow range of sizes, incompatible with the large ($L \gtrsim R_*$) tenuous loops claimed by previous analyses of flares on AD Leo and other similar stars. The flaring loops appear to have a larger cross section ($\beta = r/L \simeq 0.3$) than customarily assumed (e.g. $\beta \simeq 0.1$). All flares show evidence of significant heating during the decay phase. Although the derived peak pressures are high (up to $P \simeq 10^4$ dyne cm^{-2}) with a peak temperature of $\simeq 50$ MK, the magnetic fields required to confine such loops and to produce the observed flare luminosity are relatively modest ($B \simeq 1$–2 kG) and fully compatible with the photospheric magnetic fields measured in several flare stars. If the narrow range of loop sizes obtained is extrapolated to the quiescent structures responsible for the active corona, the latter can be naturally scaled up from the solar case through a modest (a factor of 10) increase in pressure in otherwise solar-like active structures with a small surface filling factor ($\simeq 5\%$). The quiescent component of the corona shows no evidence for abundance peculiarities with respect to the photosphere, and the quiescent coronal luminosity is remarkably constant (with variations of less than a factor of 2) across the almost 20 yr span of the observations discussed here.

Key words: stars: individual: AD Leo – stars: late-type – stars: activity – stars: coronae – X-rays: stars

1. Introduction

While the solar analogy is almost universally accepted as the starting point for the modeling of stellar coronae, its scaling to the much higher activity levels seen in active stars is still a debated question. The Sun displays, even at the maximum of its 11 year cycle, a rather low level of activity, when compared to the most active stars; dMe dwarfs (flare stars) on the other hand exhibit quiescent activity levels which are up to three orders of magnitude higher (in terms of the surface flux) than the Sun at minimum, and still a factor of hundred higher when compared with the Sun at maximum.

If the solar corona is considered in an integrated fashion (as one has to do for unresolved stellar sources) different areas of the Sun will dominate the spectrum depending on the band of interest. Orlando et al. (2000) have for example examined the Sun in an intermediate activity state, showing that active regions (defined as regions whose X-ray surface luminosity in the Yohkoh/SXT thin aluminum filter is at least 1% of the peak surface luminosity of the Sun at the given time) occupy only 2–3% of the solar surface, with the rest of the solar surface covered with low surface-brightness structures (quiet regions). Given that the active regions have significantly higher temperatures than the quiet regions, they dominate the spectrum at different energies: notwithstanding their very low surface brightness, quiet regions still dominate the integrated spectrum below $\simeq 0.5$ keV, while the few (seven in the case examined by Orlando et al. 2000) active regions dominate the spectrum at energy $\gtrsim 0.5$ keV, where the quiet regions are essentially invisible (Peres et al. 2000). The active regions dominating the emission above $E \simeq 0.5$ keV have characteristic sizes (loop semi-lengths) $L \lesssim 0.2\ R_\odot$ (e.g. Mewe 1992 and reference therein).

Several options are in principle available for scaling the solar corona up to the much higher X-ray luminosity seen in very active stars. One possibility is to augment the surface filling factor of the active region structures, up to complete coverage of the solar surface, without significantly changing their characteristics (size and pressure). This would lead to a maximum possible increase in the X-ray luminosity of a factor of approximately 100, thus naturally explaining the X-ray luminosity ($\simeq 5 \times 10^{28}$ erg s^{-1}) of intermediate-activity solar-type stars (as discussed in detail by Drake et al. 1999). To explain the higher X-ray luminosity (up to few times 10^{30} erg s^{-1}) observed in the most active solar-type stars different mechanisms must be at work. The coronal structures must either be significantly larger than in the solar case, and/or the plasma pressure

Send offprint requests to: F. Favata
Correspondence to: ffavata@astro.estec.esa.nl

must increase. Large coronal structures ($L \gtrsim R_*$) are implied by the results of several studies of the decay phase of stellar flares. If the active regions of X-ray luminous stars are so large, the increase in available volume, together with a high volume filling factor, could indeed lead to the higher X-ray luminosities observed in the most active stars without significantly increasing the plasma pressure – and the observed saturation could be explained in terms of a maximum coronal volume filling factor. At the same time, however, increasing the coronal pressure n is – given that the X-ray emissivity of the plasma at typical coronal temperatures scales as n^2 – a highly effective way to increase the X-ray luminosity.

The question of the scaling of the corona to higher X-ray luminosity is relevant to stellar evolution in general: higher-pressure structures imply larger confining magnetic fields, which in turn will have an influence on the convection region (magnetic fields modify the heat-transport capacity of the convective envelope), and thus on the structure of the star as such. High internal magnetic fields may even prevent a low-mass star from becoming fully convective. The structure of the magnetic field will also have an influence on the loss of angular momentum through magnetic braking, and thus again on the evolution of the internal structure of the star, as well as, likely, on the depletion pattern of light elements (Ventura et al. 1998a). Finally, the issue of whether the frequent and intense flares seen in very active stars are produced within closed coronal structures (as opposed to the production of intense flares in freely expanding plasmoids, i.e. large-scale coronal mass ejections) is relevant to the question of the contribution of the plentiful low-mass flare stars to the chemical evolution of our Galaxy.

Lacking spatial resolution, no direct information about the size of coronal structures can be obtained for stars (although this is sometimes possible for eclipsing binaries, see Schmitt 1998 and Schmitt & Favata 1999). The upcoming generation of high spectral resolution X-ray missions (*Chandra* and XMM) will offer the possibility of direct measurements of density-sensitive spectral diagnostics at different coronal temperatures, and thus of estimating (using the differential emission measure determination from the line fluxes) the volume of the emitting region as a function of temperature. Even with these large-area X-ray observatories, however, only a limited number of bright sources will yield enough photons to produce sufficiently high S/N spectra. For the most part, thus, information about the structuring of the corona on the majority of active stars will still have to rely, for the foreseeable future, on indirect methods.

The study of the decay phase of stellar flares is up to now the main available tool for the determination of the characteristic sizes of coronal structures, although in principle it only gives information about the flaring regions. While many flares have been studied in these terms, most studies have been limited to the analysis of individual flaring events, whose size may well be peculiar and not representative of the typical scales of the corona as a whole, and in particular of its quiescent structures. For the few stars for which a significant number of flares has been observed, a systematic, homogeneous study can provide a more general view of the the characteristic sizes of coronal structures; based on the solar analogy, where the same active regions which dominate the high-temperature emission measure are responsible for the flares, the flaring loops can then be used, qua size, as proxies for the active corona as a whole.

Table 1. The main characteristics of the *Einstein* IPC, ROSAT PSPC and ASCA SIS detectors (spectral band and resolution), together with the main features of the AD Leo observation performed by each of them (exposure time, elapsed time, number of analyzed flaring events).

	Band keV	Resolution eV at 1 keV	$t_{\rm exp}$ ks	$t_{\rm ela}$ ks	N. flares
IPC	0.16–3.5	1000	18.4	145	1
PSPC	0.1–2.0	450	22.5	60	2
SIS	0.5–10.0	100	87.0	240	3

In the present paper we undertake such systematic study on the flare star AD Leo (a dM3e star whose characteristics are discussed in detail in Appendix A), an ideal target given its high X-ray flux and the significant number of flares observed thus far. The flares we analyze here have been observed by three different instruments (*Einstein* IPC, ROSAT PSPC and ASCA SIS), with different bandpasses and energy resolution. The different bandpasses allow to explore events across a range of peak temperatures; if the characteristics of the flaring loops thus derived are similar, this is a strong indication of the corona being dominated by a class of structures. We have coherently analyzed all the AD Leo flares with sufficient statistics; the main result is that all six flares originate from similar, compact structures. Assuming that the loops which are responsible for the flares are also the main constituent of the active corona, we then constrain its characteristics, in particular regarding the filling factor and the coronal pressure. The paper is structured as follows: Sect. 2 describes the observations and their reduction, the analysis of the individual flares is discussed in Sect. 3 (with specific details about the analysis of the *Einstein* IPC flare in Appendix B), the results are discussed in Sect. 4, while Sect. 5 contains the conclusions.

2. Observations and data reduction

AD Leo has been observed on several occasions both in the X-ray and UV (as described in Appendix A.1). In the present paper we have analyzed the *Einstein*, ROSAT and ASCA X-ray observations, in all of which significant flaring events were detected. Table 1 shows a summary comparison of the characteristics of the different detectors, observations and number of flaring events studied in each. All of the observations discussed here were retrieved from the HEASARC archive, and were analyzed using the FTOOLS 4.1 software suite (except for the PSPC flaring spectra which were analyzed using the PROS package). Spectra and light curves were extracted with the XSELECT package and the spectral analysis was performed using the XSPEC 10.0 package and the MEKAL plasma emission model (Mewe et al. 1995), with (when necessary) an interstellar absorption components following the Morrison & McCammon (1983) model. To allow the comparison of results obtained with different instruments

we will quote all X-ray luminosities both in the instrument's "own" band and in a common 0.5–4.5 keV band.

2.1. The Einstein *IPC observation*

AD Leo was, on May 13 1980 (starting at 11:14 UT), the target of a long IPC observation (18.4 ks effective exposure, $\simeq 145$ ks elapsed time). This observation was briefly discussed by Ambruster et al. (1987), who noted the presence of "a previously unreported flare", and showed that no significant time variability is present before the flare, while after the event significant variability is seen on time scales of $\gtrsim 100$ s. The light curve of the observation is plotted in Fig. 1: the large flare near the beginning of the observation, with an enhancement of a factor of approximately 7 in count rate, is evident.

Somewhat curiously, given that this is the most intense event observed by the IPC on a flare star, it has never been analyzed previously (nor to our knowledge reported, apart from the brief mention of Ambruster et al. 1987). Schmitt et al. (1990), in their systematic analysis of all stellar IPC spectra, note that the spectrum cannot be fit with any of the models they considered – i.e. one- or two-temperature models or continuous emission measure models – most likely because of the presence of the flaring emission.

We have extracted the spectra (both quiescent and flaring) from a 3 arcmin radius circle centered on the source, and analyzed the "quiescent" spectrum extracted in the four segments at around 50 ks from the beginning of the observation. The background was extracted from a ring with internal and external radii of 3.5 and 5 arcmin. We have, in keeping with the photospheric metallicity and with the ASCA results, frozen the coronal metallicity to $0.2\ Z_\odot$; no absorbing column density is necessary to fit the spectrum. The resulting quiescent X-ray luminosity is $L_{\rm X} = 4.4 \times 10^{28}$ erg s^{-1} in the *Einstein* 0.16–3.5 keV band (and 3.2×10^{28} erg s^{-1} in the 0.5–4.5 keV band) with coronal temperatures of 0.3 and 8.5 MK.

2.2. The PSPC observation

AD Leo was observed by the ROSAT PSPC in pointed mode on May 8 1991, for a total effective exposure of 22.5 ks and a time span of $\simeq 60$ ks. The light-curve (binned in 120 s intervals) is shown in Fig. 2: variability is evident on several time scales, although a quiescent level of $\simeq 3$ PSPC cts s^{-1} can be identified near the middle of the observation. At least two individual flaring events can be recognized, one starting at $\simeq 28$ ks from the beginning of the observation and another, longer event starting at $\simeq$ 73 ks, with both rise and decay visible for the second flare. The average spectrum during the complete observation has been analyzed both by Giampapa et al. (1996) and Sciortino et al. (1999), as discussed in Appendix A.1 For the purpose of the flare analysis, source photons have been extracted from a circular region 3 arcmin in diameter, and the quiescent spectrum has been obtained from the segment between 60 and 65 ks, where no flaring activity is evident.

2.3. The ASCA observation

The ASCA observation of AD Leo discussed in the present paper[1] was a performed starting on May 3 1996 01:35 UT for a total elapsed time of $\simeq 240$ ks, and an on-source time of $\simeq 87$ ks. Source photons have been extracted, for both SIS-0 and SIS-1 detectors, from a circular region 3.7 arcmin in radius (36 pixels) centered on the source position, while background photons have been extracted from the whole CCD chip excluding a circular region 5.7 arcmin in radius, also centered on the source. The SIS-1 background-subtracted light curve for the complete ASCA observation (binned at 150 s intervals) is shown in Fig. 3.

While the first part of the observation is characterized by a relatively constant light curve, with little variation, significant variability is present starting at $\simeq 80$ ks from the beginning of the observations. Several individual flaring events can be recognized, in particular one starting at $\simeq 80$ ks (flare 1), one starting at $\simeq 100$ ks (flare 2) and one starting at $\simeq 107$ ks (flare 3). After the flaring activity the light curve is characterized by a much higher level of variability than before, with variations in the source count rate of a factor of $\simeq$ 2–3 on time scales of tens of ks evident toward the end of the observation, i.e. comparable to the enhancements observed for the two PSPC flares we have analyzed. Such flares have too limited statistics to allow analysis from the ASCA data; the observation shows however that they are frequent.

2.3.1. The quiescent emission in the ASCA data

The first part (up to $\simeq 80$ ks elapsed time) of the ASCA observation is characterized by a flat light curve, showing little variability, which allows to study in detail the quiescent coronal emission from the star. For this purpose, we have extracted spectra for both the SIS-0 and the SIS-1 detectors for the time interval 0–82 ks from the beginning of the observation, and fit it with a two-temperature MEKAL spectrum. Given the distance to AD Leo, the interstellar column density is expected to be small ($< 10^{19}$ cm^{-2}), with no influence on the SIS spectra. Spectra have been rebinned in energy to variable-size bins containing each at least 20 cts, and Gehrels statistics have been used in XSPEC to compute the reduced χ^2. The SIS-0 and SIS-1 spectra have been fit simultaneously to the same source model.

A simple two-temperature fit with abundance ratios fixed to the solar value converges to $[{\rm Fe/H}] = -0.77$, but fails to yield a satisfactory fit, with $\chi^2 = 1.51$ over 158 degrees of freedom, corresponding to a probability level of $\simeq 10^{-5}$. Inspection of the spectrum (left panel of Fig. 4) shows the presence of a strong line complex at $E \simeq 1.8$ keV, which is significantly underpredicted by the model, plus some excess around $E \simeq 0.6$ keV. Given that the line is at the energy of the Si K complex, while the low-energy excess is close to the O K complex energy, we

[1] ASCA also observed AD Leo in 1993, in a 2-CCD mode, in which the source fell very close to the gap between the two chips, making the spectral analysis difficult. The quiescent level during was very similar to the 1996 observation, and a small flare is present near the end. We will not further consider the 1993 observation.

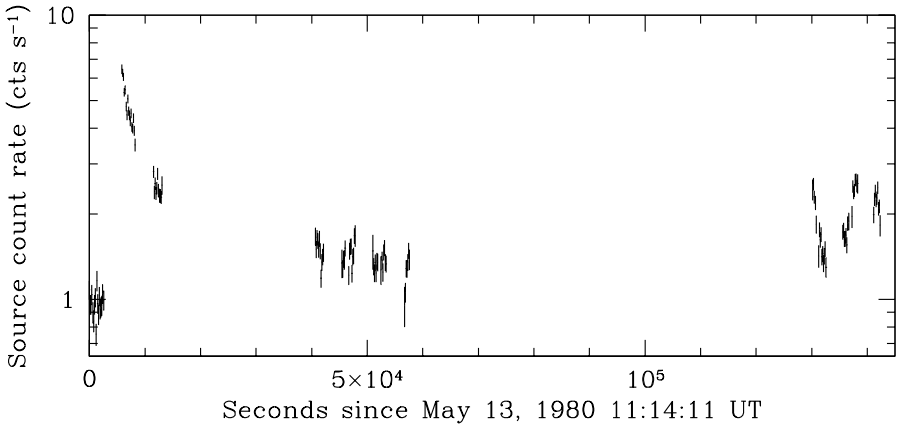

Fig. 1. The light-curve of AD Leo in the *Einstein* IPC observation, background-subtracted (background count rate $\simeq 0.087$ cts s^{-1}) and binned in 150 s intervals.

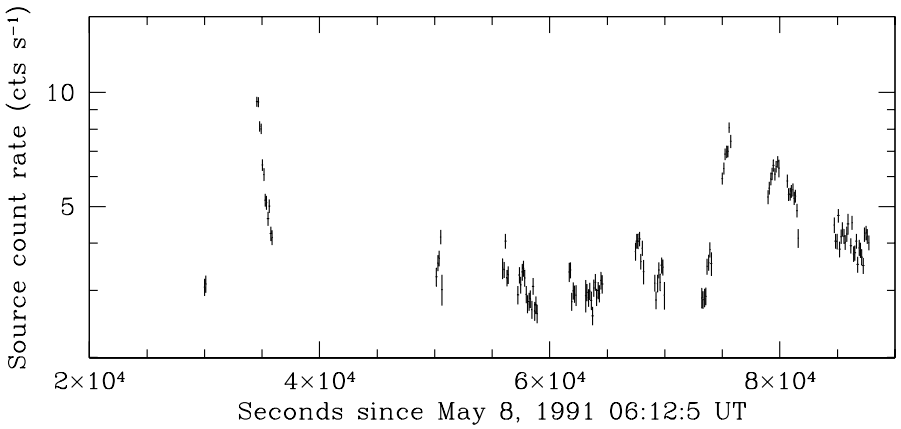

Fig. 2. The light-curve of AD Leo in the PSPC observation, background-subtracted (background count rate $\simeq 0.061$ cts s^{-1}) and binned in 120 s intervals.

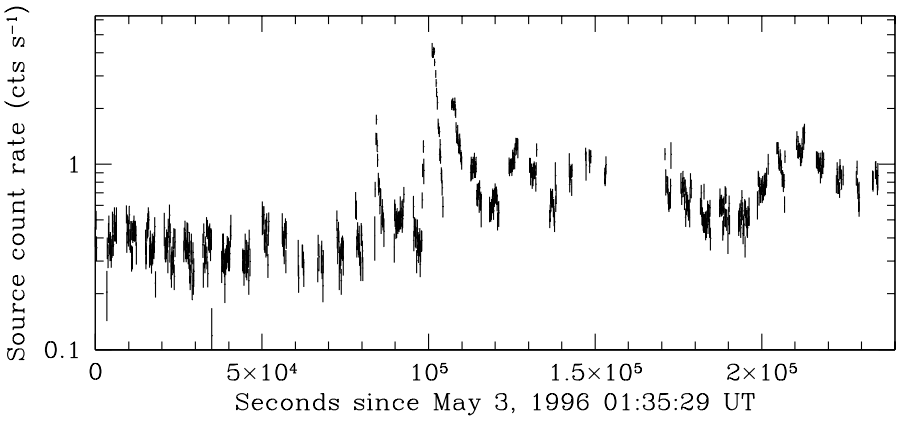

Fig. 3. The light-curve of AD Leo for the ASCA observation, as seen by the SIS-1 detector, background-subtracted (background count rate $\simeq 0.025$ cts s^{-1}) and binned in 150 s intervals.

have fit the data with a two-temperature MEKAL model, with Si and O abundances decoupled from the other abundances. The resulting model (shown in the right panel of Fig. 4) does indeed produce an acceptable fit (reduced $\chi^2 = 0.96$, corresponding to a probability level of $\simeq 60\%$). The Si line is now well fit, and the low-energy excess is reduced. The coronal Fe abundance is $[\mathrm{Fe/H}] = -0.68$, while the both O and Si are $\simeq 2.5$ times over-abundant with respect to the solar abundance ratios. The fit is not sensitive to changes in the abundance ratios of the other α elements which might contribute to the X-ray spectrum, i.e. Mg, S and Ca. The best-fit model parameters with relevant confidence ranges are shown in Table 2. The quiescent X-ray luminosity is $L_{\mathrm{X}} = 5 \times 10^{28}$ erg s^{-1} in both the instruments own 0.5–10 keV band and in the 0.5–4.5 keV band.

3. Flare analysis

Various approaches have been developed for the analysis of stellar flares, in general based on some physical model of the flaring region and a fit of the observed decay behavior to the model, to derive the "best-fit" physical parameters. Most of these models assume that the flare decay is dominated by the characteristics of the flaring region, with negligible sustained heating during the decay phase. Among these are the quasi-static method[2], first

[2] In principle the quasi-static formalism, as originally developed, would allow to include sustained heating. However, also due to the mathematical complexity of the formulation, it has generally been applied assuming free decay of the loop.

Table 2. The spectral parameters derived for the quiescent emission of AD Leo from the analysis of the SIS-0 and SIS-1 spectra accumulated during the first part of the ASCA observation (i.e. up to 82 ks elapsed time) using a two-temperature MEKAL spectral model. The first row shows the results of a fit with abundance ratios fixed to the solar values, while the second row shows the best-fit model with O and Si abundance decoupled from the rest. The quiescent X-ray luminosity corresponding to the spectral parameters shows is 5×10^{28} erg s^{-1} (both in the 0.5–10 keV and in the 0.5–4.5 keV bands). Quoted uncertainties correspond to $\Delta\chi^2 = 2.7$.

T_1	T_2	EM_1	EM_2	[Fe/H]	[O/H]	[Si/H]	χ^2	DoF
keV		10^{50} cm^{-3}						
0.37 ± 0.03	0.87 ± 0.03	28 ± 1	30 ± 1	-0.77 ± 0.03	$= [\mathrm{Fe/H}]$	$= [\mathrm{Fe/H}]$	1.51	158
0.48 ± 0.08	0.85 ± 0.05	16 ± 3	23 ± 6	-0.68 ± 0.08	-0.27 ± 0.07	-0.28 ± 0.08	0.96	156

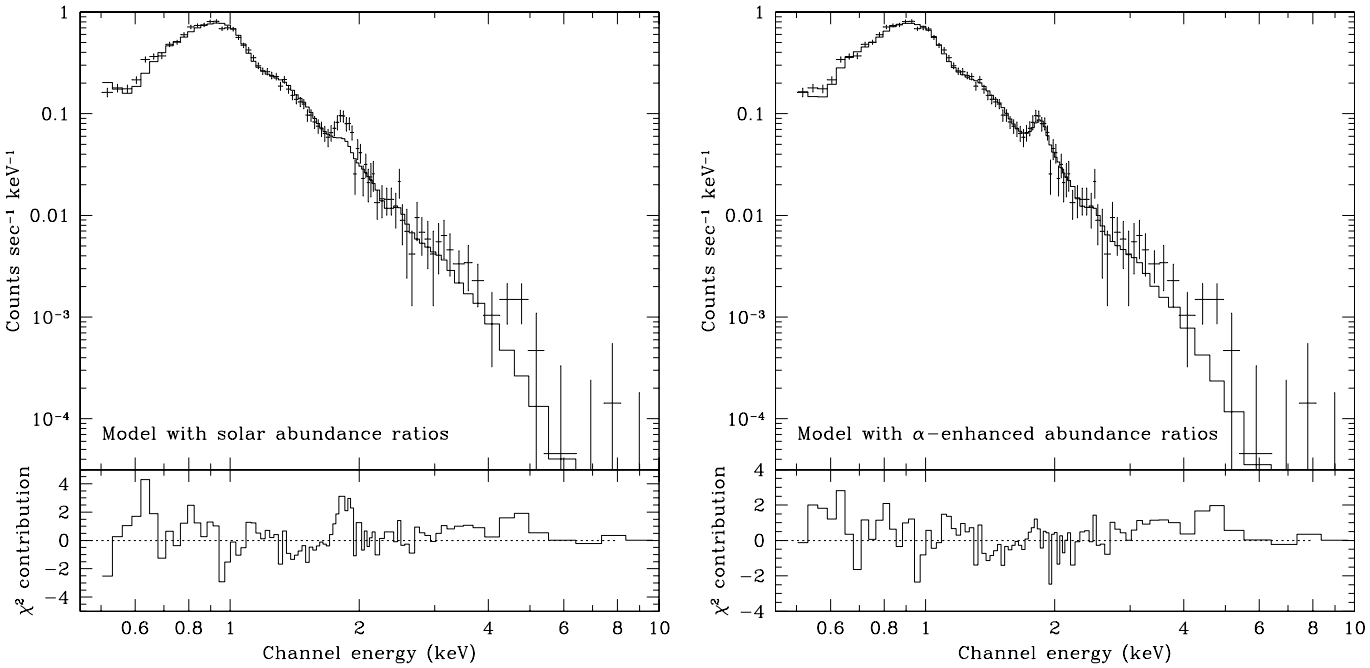

Fig. 4. Quiescent SIS spectra of AD Leo (only the SIS-0 spectrum is shown for clarity). The left panel shows the observed spectrum together with a best-fit two-temperature MEKAL model with all the abundances varying in lockstep (best fit $[\mathrm{Fe/H}] = -0.77$), while the right panel shows a two-temperature MEKAL model with the O and Si abundance decoupled from the other abundances, with $[\mathrm{Fe/H}] = -0.68$ and $[\mathrm{O/Fe}] \simeq [\mathrm{Si/Fe}] \simeq 0.4$.

applied by van den Oord & Mewe (1989) for a flare on Algol, and the method of Fisher & Hawley (1990), applied for example to the analysis of a flare seen by EUVE on AD Leo itself (Cully et al. 1997). This type of approach has been employed in the literature for the analysis of several flaring events, as have simpler scaling arguments again based on the assumption of freely decaying loops; in general, these analyses, when applied to intense, long-lasting events naturally result in long ($L \gtrsim R_*$) tenuous loops.

Reale et al. (1997) have developed an approach to the analysis of the decay phase of flares based on detailed hydrodynamic modeling of decaying flaring loops with explicit allowance for sustained heating (parameterized as an exponential function of time) during the decay phase. The method uses as a diagnostic for presence of heating during the decay phase the slope of the locus of the decay in the $\log n$–$\log T$ plane (Sylwester et al. 1993). An extensive set of hydrodynamic models of decaying flaring loops has made it possible to derive empirical relationships between the light curve decay time (in units of τ_{th}, the loop thermodynamic decay time, Serio et al. 1991) and the slope ζ of the flare decay in the $\log n$–$\log T$ diagram (using the square root of the emission measure of the flaring plasma as a proxy to the density).

Application of this approach to the Sun has shown that sustained heating during the flare decay is common in solar events (Reale et al. 1997); when stellar events are analyzed within this framework, the resulting loop sizes are invariably significantly smaller ($L < R_*$, i.e. "solar-like") than when the same events are analyzed as "freely decaying". We have previously applied the sustained heating framework to the analysis of flaring events on PSPC flares observed on the dMe stars CN Leo and AD Leo itself (Reale & Micela 1998), on a large flare observed by SAX on the active binary system Algol (Favata & Schmitt 1999) and on an exceptional flare observed on the dMe dwarf EV Lac by ASCA (Favata et al. 2000), with the aim of determining the characteristic sizes of coronal structures on different types

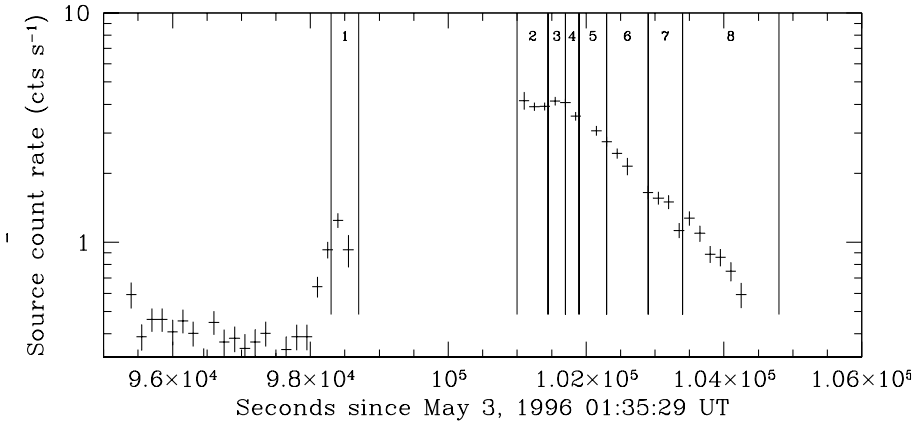

Fig. 5. The light curve of the second flare ("flare 2") observed by the ASCA SIS on AD Leo, background-subtracted (background count rate $\simeq$ 0.025 cts s^{-1}) and binned in 150 s intervals. Also shown is the extent of the time intervals from which the spectra which have been used for the determination of the flare's spectral parameters have been extracted.

of active stars. In all cases, these turned out to be compact ($L \lesssim 0.5\ R_*$), with evidence for significant sustained heating, so that the much longer loops ($L > R_*$) implied by the analyses based on the free decay approach appear to be unrealistic.

We use the Reale et al. (1997) approach to analyze all the flares discussed here. The empirical relationship between ζ and $\tau_{\rm LC}/\tau_{\rm th}$ needs to be derived separately for each X-ray detector, as it will depend on the spectral response. The loop length is a function of the maximum observed temperature during the flare $T_{\rm max}$ and of the intrinsic thermodynamic decay time $\tau_{\rm LC}$ determined from the observed decay time $\tau_{\rm th}$ and from ζ, as shown in detail for the ASCA SIS detector in Sect. 3.1. For instruments with limited spectral resolution (such as the ROSAT PSPC and the *Einstein* IPC) Reale & Micela (1998) have developed an approach based on a principal component decomposition of the spectrum, which allows optimal use of low-resolution data.

3.1. Analysis of the ASCA flares

To analyze the flares seen with the ASCA-SIS detector we have first recalibrated the method of Reale et al. (1997) for use with the ASCA SIS detectors, and in particular the empirical relationship between the observed and intrinsic decay time as a function of the slope ζ in the $\log n$–$\log T$ diagram.

The intrinsic decay time $\tau_{\rm th}$ of a closed coronal loop with semi-length L, and maximum temperature $T_{\rm max}$ is given by Serio et al. (1991) as:

$$\tau_{\rm th} = \frac{\alpha L}{\sqrt{T_{\rm max}}} \tag{1}$$

where $\alpha = 3.7\ 10^{-4}$ cm^{-1}s^{-1}K$^{1/2}$. By means of a grid of hydrostatic loop models (see Reale & Micela 1998) we have found an empirical relationship which links the loop maximum temperature $T_{\rm max}$, typically found at the loop apex (e.g. Rosner et al. 1978) to the maximum temperature $T_{\rm obs}$ determined from the SIS spectrum:

$$T_{\rm max} = 0.077 \times T_{\rm obs}^{1.19} \tag{2}$$

The ratio between $\tau_{\rm LC}$, the observed e-folding time of the flare's light curve (determined by fitting the light curve from the peak of the flare down to the 10% of peak level) and the thermodynamic decay e-folding time $\tau_{\rm th}$ is linked to the slope ζ in the $\log\sqrt{EM}$–$\log T$ diagram by

$$\frac{\tau_{\rm LC}}{\tau_{\rm th}} = F(\zeta) = c_a e^{-\zeta/\zeta_a} + q_a \tag{3}$$

where the constants are, for the ASCA SIS detector, $c_a = 61$, $\zeta_a = 0.035$ and $q_a = 0.59$. The formula for the loop semi-length L is therefore:

$$L = \frac{\tau_{\rm LC}\sqrt{T_{\rm max}}}{\alpha F(\zeta)} \qquad 0.4 < \zeta \leq 1.7 \tag{4}$$

where the second part of the relationship gives the range of ζ values allowed according to the modeling. The uncertainty on L comes both from the propagation of the errors on the observed parameters $\tau_{\rm LC}$ and ζ and from the uncertainty intrinsic to the modeling, i.e. the ability of Eq. (4) to reproduce the true length of the modeled loops. From the self-consistency checks the latter error amounts to $\simeq 18\%$.

We have applied the above approach to the three flares visible in the ASCA light curve of AD Leo; for each of them the light-curve has been subdivided in time intervals containing $\simeq 1000$ cts per SIS spectrum, as shown in Fig. 5 for the second event. The SIS-0 and SIS-1 spectra from each of these events have been simultaneously fit with a one-temperature MEKAL model with freely varying parameters, plus a two-temperature MEKAL model with parameters fixed at the best-fit values for the quiescent emission. An example of the resulting fit is shown in Fig. 6, for the spectrum at the peak of the SIS flare 2. The abundance for the flaring component was fixed at the same value as for the quiescent component (including the same level of α element enhancement), and best-fit temperatures and emission-measures have been derived. The limited statistics of the individual flaring spectra do not allow for the metal abundance of the flaring components to be separately determined. If it is left as a free parameter the resulting confidence range is too wide to yield useful information, and is in each case compatible with the quiescent abundance.

3.1.1. ASCA flare 1

For the first of the three ASCA flares too few source photons are available to allow a complete analysis. With a peak count

Table 3. The spectral parameters T and EM derived for the individual phases of the second flare in the AD Leo ASCA observation from the analysis of the SIS spectra. The spectra have been analyzed with a single-temperature model (plus a frozen-parameter two-temperature model to account for the quiescent emission). The bounds of the confidence intervals (at $\Delta\chi^2 = 2.7$) are also reported for each parameter. The time interval i to which each set of parameters applies is shown in Fig. 5.

i	T	$T_{-90\%}$	$T_{+90\%}$	EM	$EM_{-90\%}$	$EM_{+90\%}$	χ^2	DoF	Prob.
		keV			10^{50} cm^{-3}				
1	2.12	1.48	3.44	84.8	68.3	100.6	0.95	25	0.53
2	1.27	1.19	1.36	509.9	484.4	535.6	1.24	71	0.08
3	1.33	1.24	1.43	501.5	476.8	526.1	1.32	78	0.03
4	1.31	1.21	1.43	471.6	444.9	498.7	1.15	61	0.20
5	1.10	1.03	1.18	361.1	339.6	382.8	1.23	59	0.11
6	1.09	1.02	1.17	276.1	260.3	292.0	1.07	65	0.33
7	1.00	0.91	1.09	139.0	128.5	149.6	1.28	55	0.08
8	0.78	0.71	0.85	70.89	64.3	77.5	0.83	61	0.83

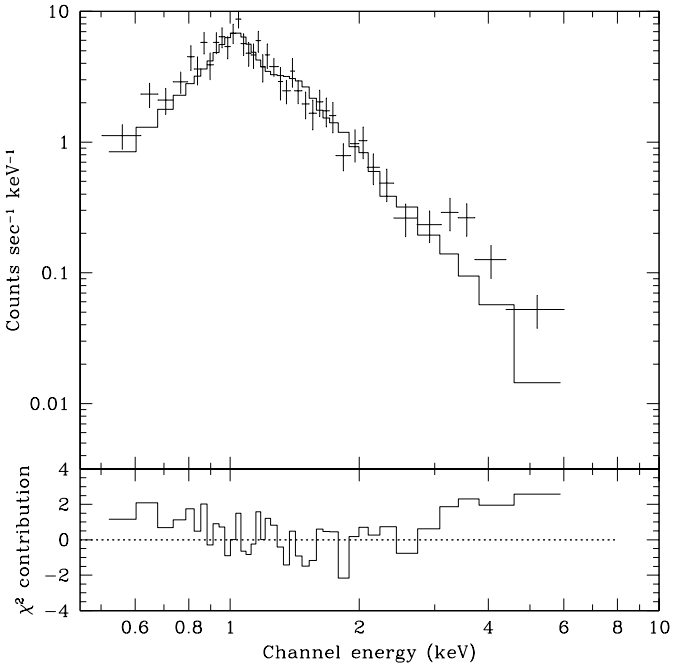

Fig. 6. The SIS-0 spectrum of AD Leo at the peak of flare 2 (time interval 2 in Fig. 5), plotted together with the best-fit MEKAL isothermal model fit to the flaring emission.

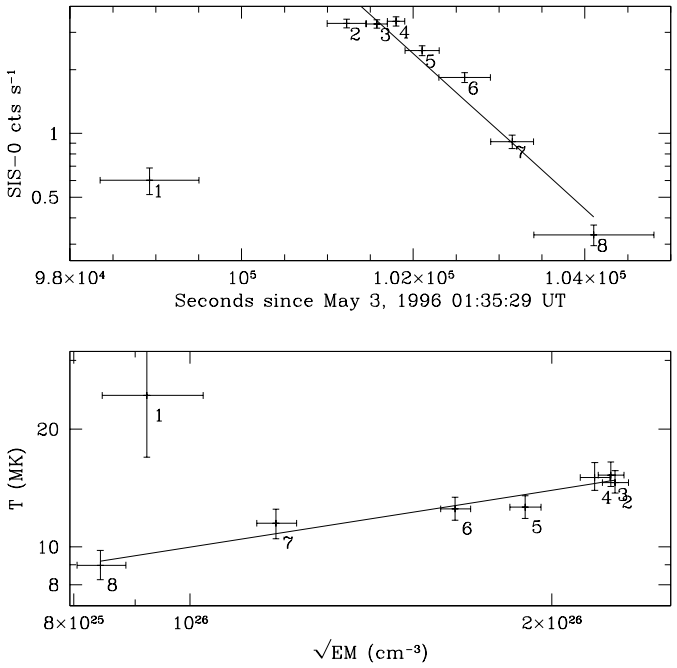

Fig. 7. The top-panel shows the temporal evolution of the light-curve of the second flare seen in the SIS light-curve (flare 2), binned in intervals containing $\simeq 1000$ SIS counts, together with the best-fit exponential decay to the light-curve (yielding an e-folding time of 1180 ± 130 s). The bottom panel shows the T versus $\sqrt{EM}$ plot for the same time intervals. The flare decay slope in this plane is $\zeta = 0.48 \pm 0.06$.

rate of $\lesssim 2$ cts s^{-1} and a decay time scale $\tau_{\rm LC} \simeq 570$ s, it is not possible to follow the decay of the event in the $\log\sqrt{EM}$–$\log T$ plane. The peak temperature for the event is $\simeq 20$ MK. An upper limit to the loop size can be obtained through Eq. (4) by assuming that the influence of sustained heating is negligible (i.e. $F(\zeta) \simeq 1$). Under this assumption, $L < 10^{10}$ cm. The peak X-ray luminosity for the event is 9×10^{28} erg s^{-1}.

3.1.2. ASCA flare 2

The second flaring event, the better defined of the three, has sufficient source counts to allow a detailed analysis and to constrain rather narrowly the characteristics of the flaring region. Its light-curve is shown in Fig. 5, where the intervals in which the flare has been subdivided for the spectroscopic analysis are shown.

The evolution of the flare in the $\log\sqrt{EM}$–$\log T$ plane is shown in the lower panel of Fig. 7, together with a least-square fit to the decay phase. The resulting best-fit slope is $\zeta = 0.48 \pm 0.06$. The top panel of Fig. 7 shows the light curve binned in the same intervals as used for the spectral analysis, together with the best-fitting exponential decay (with an e-folding time $\tau_{\rm LC} = 1180 \pm 130$ s).

Application of Eq. (3) yields a ratio between the observed cooling time scale $\tau_{\rm LC}$ and the thermodynamic cooling time

scale for the flaring loop $\tau_{\rm th}$ of $F(\zeta) = 5.4$, indicative of the presence of strong sustained heating, and showing that the observed decay is driven by the time-evolution of the heating process and not by the spontaneous decay of the loop. As $\tau_{\rm LC} = 1.18 \pm 0.13$ ks, $\tau_{\rm th} \simeq 220$ s. The intrinsic flare peak temperature is, applying Eq. (2) to the observed maximum temperature, $T_{\rm max} \simeq 48$ MK. From Eq. (4) the loop semi-length is then $L = (4.1 \pm 1.0) \times 10^9$ cm, i.e. $L \simeq 0.15\ R_*$. This loop length is much smaller than the pressure scale height[3] $H \simeq 3 \times 10^{11} \simeq 11\ R_*$.

The peak X-ray luminosity of the flare is $\simeq 2.5 \times 10^{29}\ {\rm erg\ s^{-1}}$ in either the 0.5–10 keV or the 0.5–4.5 keV band, and the total energy radiated in X-rays by the flare (obtained by simply integrating the X-ray luminosity in each of the intervals in which the flare has been subdivided) is $\simeq 3.2 \times 10^{31}$ erg. Using the same simple argument discussed by Favata et al. (2000) we can estimate the magnitude of the magnetic field necessary to confine the loop and to produce the energy (presumably by magnetic recombination) radiated in the flare. The magnetic field required to confine the flaring plasma (which has a maximum pressure of $\simeq 2 \times 10^4$ dyne cm^{-2}) is $B \simeq 0.6$ kG, while the minimum magnetic field required to explain the flare energetics is $B \simeq 1.4$ kG. Such fields are relatively modest, and fully compatible with the values of few kG with large filling factors measured e.g. by Johns-Krull & Valenti (1996) in a few active M dwarfs with characteristics similar to AD Leo.

3.1.3. ASCA flare 3

The decay of the third flare is more irregular than for flare 2, and with a lower statistics (given that the peak count rate is a factor of $\simeq 2$ lower), resulting in a much larger range for the slope T versus $\sqrt{EM}$ plot, and thus in a much larger confidence region for the estimate of the loop length. The nominal observed decay time is $\tau_{\rm LC} \simeq 3500$ s, and the peak temperature is 38 MK. Also in this case there is evidence for strong sustained heating (with $\zeta \simeq 0.4$, at the limit of validity of the method, implying $\tau_{\rm LC}/\tau_{\rm th} \simeq 8$), and the resulting loop size is compatible with the one derived for flare 2, at $\simeq 7 \times 10^9$ cm, with a $1\,\sigma$ uncertainty of a factor of $\simeq 2$. The intrinsic decay time is, at $\tau_{\rm th} \simeq 400$ s, similar to the one of flare 2. The compatible loop size, together with the temporal proximity of the two events is in principle consistent with the two (or even three) flares coming from the same loop, repeatedly heated. However, "sympathetic flaring", as observed in the Sun is also a possibility.

3.2. The PSPC flares

The first PSPC flare (as reported by Reale & Micela 1998) has a short decay time $\tau_{\rm LC} = 680$ s, with evidence for moderate sustained heating ($F(\zeta) \simeq 2.5$), so that the loop intrinsic decay time is $\tau_{\rm th} \simeq 300$ s, very similar to the decay time of the better defined of the events analyzed here (the ASCA flare 2). The loop length derived by Reale & Micela (1998) is $L \simeq 4 \times 10^9$ cm, with $\simeq 60\%$ uncertainty. The peak temperature is $\simeq 35$ MK.

For the purpose of the analysis the light-curve of the second flare (which we analyze in the present paper) has been subdivided in 5 intervals, of duration 1, 1, 1, 1.2 and 1.7 ks. The event is a long-lasting one, with $\tau_{\rm LC} \simeq 8.6$ ks (i.e. the longest among the events analyzed here); the slope of the flare decay is in this case $\zeta_{\rm PC} = 1.8$, outside the domain of validity of the method (see Reale & Micela 1998), and implies $\tau_{\rm H} \gg \tau_{\rm lc}$, i.e. the decay is totally dominated by the heating profile, while the effects of the loop decay are negligible. The intrinsic characteristics of the flaring loop are thus "hidden" by the time evolution of the heating, and cannot be effectively constrained by studying the decay light-curve. It is however still possible to derive an upper limit to the loop's size: the uncertainty on $\zeta_{\rm PC}$ is large (due to the irregular decay of the event, with visible evidence for reheating events, during which the count rate rises again during the decay phase), and its upper bound enters among the allowed range of values for $\zeta_{\rm PC}$, allowing to derive an upper limit, $L < 17 \times 10^9$ cm, still well below the pressure scale height.

3.3. The Einstein *IPC flare*

We have analyzed this long-lasting event with the same approach as the one described by Reale & Micela (1998) for flares observed with the PSPC detector, but tuned for the IPC detector (the details are described in Appendix B). The light-curve of the flare (i.e. the second and third observation segments visible in Fig. 1) has been divided, for the purpose of the analysis, in 4 intervals. Segment 2 has been subdivided in three intervals (of 600, 800 and 1060 s each), while segment 3 was considered as a single interval of 1550 s duration. The length of these intervals was chosen so to have approximately the same number of photons ($\simeq 4000$) in each spectrum. The quiescent spectrum extracted from the 2700 s pre-flare segment, properly scaled, has been subtracted from the spectra extracted from the four flaring time intervals to derive the net flare spectra.

The IPC event has an observed decay time $\tau_{\rm LC} = 5400 \pm 600$ s; our analysis again shows that significant heating is present during the decay phase, with $F(\zeta) = 3.8$, so that the thermodynamic loop decay time is $\tau_{\rm th} \simeq 1400$ s. The peak temperature is relatively low ($T_{\rm max} = 12$ MK), and the loop length is $L = (1.3 \pm 0.4) \times 10^{10}$ cm (or $0.5 \pm 0.15\ R_*$).

4. Discussion

Under the assumption of validity of the method used to derive parameters of the flaring loops (and discussed in detail in Reale et al. 1997), our comparative analysis of flares on AD Leo (whose results are summarized in Table 4), with six events observed by three different instruments, allows – together with the study of the quiescent emission as seen by the ASCA SIS – for the first time to study the characteristics of the AD Leo corona (and by extension of the coronae of flare stars) in a systematic way.

[3] defined as $H = 2kT/\mu g \simeq 6000 \times T_{\rm max}/(g/g_\odot)$, where T is the plasma temperature in the loop, μ is the molecular weight of the plasma and g is the surface gravity of the star.

Table 4. Characteristics of the various flaring events studied on AD Leo. The stellar radius is $R_* = 26 \times 10^9$ cm. For each flare we list the observed light-curve decay time, the value of $F(\zeta)$ resulting from Eq. (3), the corresponding intrinsic loop thermodynamic decay time, the loop semi-length inferred from Eq. (4), the peak temperature, the peak emission measure and X-ray luminosity (in the 0.5–4.5 keV band) and the total energy released in X-rays during the decay of the event, the pressure resulting from the application of the Rosner et al. (1978) scaling laws for the loop length and temperature derived from the flare analysis, and the loop volume, density and pressure derived from the peak EM and T and assuming a loop aspect ratio $\beta = 0.1$ (typical of solar loops). The subscript within parentheses indicates the power of 10 by which the given quantity has been scaled.

										$\beta = 0.1$		
Flare	$\tau_{\rm LC}$ s	$F(\zeta)$	$\tau_{\rm th}$ s	$L_{(9)}$ cm	$T_{\rm max}$ MK	$EM_{(50)}$ cm^{-3}	$L_{\rm X\,(28)}$ erg s^{-1}	$E_{\rm X\,(31)}$ erg	$P_{\rm RTV\,(2)}$ dyn cm^{-2}	$V_{(27)}$ cm^3	$n_{(11)}$ cm^{-3}	$P_{(2)}$ dyn cm^{-2}
SIS–1	570	> 1	< 570	< 10.0	20	140	9	13	> 3	< 60	> 5	13
SIS–2	1180	5.4	220	4.1 ± 1.0	48	510	25	82	100	4.3	34	200
SIS–3	3500	8.0	400	7.0 ± 3.5	38	250	7	16	29	22	11	56
PSPC–1	680	2.5	300	4.0 ± 2.4	35	200	18	12	40	4	20	200
PSPC–2	8040	$\gg 1$	–	< 17.0	12	80	19	25	> 0.4	$\lesssim 300$	> 1.5	> 5
IPC	5400	3.8	1400	13.0 ± 4.0	12	100	32	250	0.5	140	3	10

4.1. Physical parameters of the flaring loops

All the flares we have studied point toward the structures in the flaring component of the corona of AD Leo being confined to a rather narrow range of characteristic sizes, small in comparison with the stellar radius ($L \lesssim 0.5\ R_*$). A summary of the characteristics of each flare analyzed here is shown in Table 4. No evidence for large loops, extending out to distances of one or more stellar radii is found in any of the observations studied. The peak flare temperatures range between $T \simeq 10$ MK and $T \simeq 50$ MK, and the peak X-ray luminosity is comprised in a narrow range ($\simeq$ 1–3 $\times 10^{29}$ erg s^{-1}). The total radiated energy is $\simeq$ 1–25 $\times 10^{32}$ erg, a much larger range than the peak luminosity, due to the large range of decay times. The pressures also span two orders of magnitude, from $\simeq 100$ to $\simeq 10\,000$ dyne cm^{-2}.

The only previously published analysis of flares on AD Leo is the one of Cully et al. (1997), who studied a significant (although smaller than the event discussed here) EUVE flare, with simultaneous ground-based optical coverage. Their analysis is however based on the assumption that during the decay phase the heating rate is negligible in comparison with the natural cooling rate of the flaring loop, so that the light curve is fully dominated by the spontaneous cooling of the loop (i.e. $\tau_{\rm LC} \simeq \tau_{\rm th}$, an approximation which Hawley et al. 1995 call the "strong condensation limit") and consequently long rise and decay times require large loop lengths (Hawley et al. 1995). The EUVE spectrum alone (given the very low S/N of the continuum) does not allow to derive the coronal abundance, and thus Cully et al. (1997) derive the flare parameters under the assumption of $Z = Z_\odot$ and $Z = 0.1 \times Z_\odot$ coronal metallicity. The loop length they derive (for the first of the two flares they have observed) is $L = 4.7$–1.5×10^{10} cm (the first value is for $Z = Z_\odot$, the second for $Z = 0.1 \times Z_\odot$, as in the following), the density $n = 4$–40×10^9 cm^{-3}, the pressure $P = 10$–100 dyne cm^{-2}, with an equipartition magnetic field $B = 16$–50 G. The peak temperature is (independent of the assumed abundance) $T = 13$ MK.

The resulting loop lengths are thus significantly larger (4 to 11 times) than the lengths derived from the ASCA flare 2 (the one which gives the tightest constraint to the derived physical parameters). Although these are distinct events, and thus could in principle result from quite different types of flaring structures, it is worth nothing that for all the X-ray flares analyzed in the present paper there is evidence for substantial heating during the decay phase (with $\tau_{\rm LC}/\tau_{\rm th}$ ranging from $\simeq 2.5$ to $\simeq 8$); if these flaring events had been analyzed assuming that $\tau_{\rm LC} \simeq \tau_{\rm th}$ the resulting loop lengths would have been over-estimated by factors 2.5–8; on the assumption that the EUVE flare is of a similar class as the ones observed in X-ray it is likely that equating $\tau_{\rm th}$ to $\tau_{\rm LC}$ will lead to an over-estimate of the loop length by similar factors as in the X-ray case. The large ($L \simeq R_*$) loop sizes derived by Cully et al. (1997) for the EUVE flares would in this case be reduced to the same characteristic size ($L \simeq 0.3 \times R_*$) derived for the X-ray flares, thus again pointing to a narrowly confined characteristic size for the structures of the flaring component of the AD Leo corona.

4.2. The aspect ratio of the flaring loops

Under the assumption that the flaring loops are similar to solar loops (i.e. that their physical parameters are regulated by the same scaling laws of Rosner et al. 1978) we can derive an estimate for the ratio for the loop's cross-section radius and its length (which in the solar case is typically $\beta \simeq 0.1$, although with a wide range of observed values). This can be done by comparing the pressure derived through the scaling laws with the pressure derived from the flare's emission measure. In the former case the pressure is obtained by application of the Rosner et al. (1978) scaling law

$$T_{\rm max} = 1.4 \times 10^3 (P_{\rm RTV} L)^{1/3} \qquad (5)$$

(which can also be written as $T_{\rm max} = 6.16 \times 10^{-4} \sqrt{n_{\rm RTV} L}$) where $P_{\rm RTV}$ is the pressure at the base of the loop, and where the flare's peak temperature and emission measure are used. In the latter case a simple estimate of the density of the flaring

plasma can be obtained by dividing the peak emission measure by the volume of the flaring loop, where the volume is obtained by assuming a given value for β, so that

$$n = \sqrt{\frac{EM}{2\pi L^3 \beta^2}} \tag{6}$$

and

$$P = nkT = kT \times \sqrt{\frac{EM}{2\pi L^3 \beta^2}} \tag{7}$$

Under the assumption that the flaring loop at flare maximum is not far from a steady-state condition (i.e. that it is almost filled up with flaring plasma), the two estimates for the pressure should yield similar results. In Table 4 we report the resulting estimates for each individual flare discussed here, with the pressure and density estimates obtained under the assumption that the loops are similar to the ones observed in the solar-corona, where typically $\beta \simeq 0.1$. As it can be seen the assumption of solar-like aspect ratio loops yields pressures which are systematically larger (and thus volumes that are systematically smaller) than the pressures derived from the scaling laws. The factors range from $\simeq$ 2 (for the ASCA-2 flare) up to $\simeq$ 20 (for the IPC flare). The two can be reconciled under the assumption of higher β values, implying loops which are "fatter", with a resulting $\beta \simeq 0.3$.

The larger β, if generally applicable, implies lower densities, so that even at the peak of the largest observed flares the plasma likely remains optically thin, justifying the analysis of the spectra without any allowance for self-absorption. In the case of the large EV Lac flare discussed by Favata et al. (2000) the larger β would for example imply that the average peak density is $n \lesssim 10^{12}$ cm^{-3}.

4.3. Energetics

A simple estimate of the heating released during the flare decay can be obtained as follows: if one assumes uniform heating along the loop the scaling laws of Rosner et al. (1978) yield

$$\frac{dH}{dVdt} \simeq 10^5 \; P_{\rm RTV}^{7/6} \; L^{-5/6} \tag{8}$$

and the total heating rate at the flare maximum is therefore

$$\frac{dH}{dt} \simeq \frac{dH}{dVdt} \times V \tag{9}$$

Given that all the events analyzed here display significant heating during the decay, the heating time scale can be approximated as $\tau_{\rm H} \simeq F(\zeta) \times \tau_{\rm th} \simeq \tau_{\rm LC}$, and an approximate estimate of the total energy released during the flare decay is

$$E \simeq \frac{dH}{dt} \times \tau_{\rm LC}. \tag{10}$$

If the above analysis is applied to the flares we have studied (determining the volume on the assumption of $\beta \simeq 3$) the peak volumetric heating rates range (for the flares for which the length is determined) between $\simeq 5$ and $\simeq 50$ erg cm^{-3} s^{-1}, and both the peak total heating and the total energy released during the flare are a few times ($\simeq 3$) larger than the peak X-ray luminosity and total radiated energy, showing that radiative losses are not the dominant term in the flare energetics (similarly to what determined for the large ASCA flare on EV Lac, Favata et al. 2000).

4.4. The quiescent active corona of AD Leo

In the Sun the same general class of structures which constitute the active part of the corona produce the flares. On the assumption that this is also true in the stellar case, we can use the range of derived properties for the flaring loops of AD Leo to infer the characteristics of the quiescent active corona, and in particular to understand the scaling from the solar picture toward much higher activity levels, i.e. whether this happens (mainly) through an increase in the filling factor, in the characteristic size of the coronal structures or through an increase in the pressure of the plasma filling the loops. The simple picture of a straightforward increase in filling factor, until the star is completely covered with solar-like active regions, can rather naturally explain (as discussed in detail by Drake et al. 1999) the luminosity of "intermediate activity" stars: using Yohkoh solar images Drake et al. (1999) show that the X-ray luminosity of the solar active regions is $\simeq 6 \times 10^{26}$ erg s^{-1}, with a filling factor $f \simeq 1$–2%. Thus, by covering a solar-type star with active regions a luminosity of $\simeq 3$–6×10^{28} erg s^{-1} can be achieved. However, such scheme, while appealing in its simplicity, is in contrast with some of the available spectroscopic indicators of coronal structuring; Ventura et al. (1998b) for example have analyzed the ROSAT PSPC spectra of active solar-type stars, showing that they are compatible with an active corona being constituted by compact, high-pressure loops with filling factors of few percent (although low-pressure, larger filling factor loops are also a possible solution). Direct pressure measurements of coronal pressure have been performed on a few stars with EUVE: while low- and intermediate-activity solar-type stars show solar-like densities (e.g. ϵ Eri, $n \simeq 10^9$ to 10^{10} cm^{-3}, Schmitt et al. 1996a; Procyon, $n \simeq 3 \times 10^9$ cm^{-3}, Schmitt et al. 1996b), supporting Drake et al. (1999)'s view of an increased filling factor being responsible for higher densities, more active stars (active binaries) show evidence for much increased coronal density ($n \gtrsim 10^{13}$ cm^{-3} e.g. in 44 Boo, Brickhouse & Dupree 1998), well above the value required to explain the enhanced X-ray luminosity through an $f \simeq 1$ corona, and again implying a small f in the more active stars.

For a dMe star such as AD Leo, with a smaller surface area (by a factor of 7 with respect to the Sun) the maximum quiescent X-ray luminosity, if covered with solar-type active regions is $\simeq (4$–$8) \times 10^{27}$ erg s^{-1}, i.e. still an order of magnitude below the observed values. Thus, another mechanism needs to be postulated to explain the higher X-ray luminosity. Given the compact sizes derived here for the flaring regions (comparable in relative terms to the solar ones), there is no evidence for large loops with significant emissivity and thus for a corona ex-

tending to large distances from the star and occupying a large volume. Given the low filling factor we derive for the quiescent component (see below) the additional X-ray emissivity is therefore likely to come from an increase in plasma pressure within the same types of (relatively small) coronal structures as in solar active regions. This is also compatible with the high photospheric magnetic fields (few kG) measured in dMe stars (Johns-Krull & Valenti 1996), which can easily confine the higher pressure loops required by this picture of the corona.

Giampapa et al. (1996) have studied the ROSAT spectra and light curves of several M dwarfs (including AD Leo) with the help of semiempirical loop models. They infer that two distinct thermal components are present in the coronae of M dwarfs, a quiescent cooler one showing negligible time variability, and a hotter flaring one responsible for the observed variability. The cooler component has a characteristic temperature (in the PSPC spectra) of $\simeq 3$ MK, while the hotter one has $T \simeq 10$ MK. The cool component can be modeled in terms of small ($L \ll R_*$), high-pressure ($P \gtrsim P_\odot$) loops, while for the hotter component two classes of solutions are possible, i.e. it can be composed either of large ($L \gtrsim R_*$), high-pressure ($P \gtrsim P_\odot$) loops or of small ($L \lesssim R_*$) loops with a very high pressure ($P \gg P_\odot$) and a very small filling factor ($f \ll 0.1$). Again, the former possibility (a flaring component of the corona composed of large loops) is not supported by our analysis; this is also in agreement with the results of Sciortino et al. (1999), who have modeled the time-averaged SAX LECS and MECS spectrum of AD Leo using static loop models; they show that the observed spectrum is compatible with being emitted from compact loops ($L \lesssim 0.1\ R_*$) with a small filling factor ($f \lesssim 10^{-3}$).

In the present case the filling factor for the hotter component can be estimated under the assumption that the corona is largerly composed by loops which satisfy the scaling laws of Rosner et al. (1978) – i.e. Eq. (5) – starting from the measured quantities T, EM and L. Assuming that the loop size (parameterized as $L = \alpha \times R_*$, where $\alpha \simeq 0.3$) is now known, the emission measure is linked to the loop size and density by

$$EM = Nn^2V = Nn^2 2\pi\beta^2(\alpha R)^3 \tag{11}$$

where N is the number of emitting loops, $V = \pi\beta^2\alpha^3R^3$ is the volume of a single loop and β, as before, the aspect ratio of the loop. If the filling factor is defined as the fraction of the stellar area covered by loops, i.e.

$$f = \frac{NA}{4\pi R^2} \tag{12}$$

where $A = \pi\beta^2\alpha^3R^2$ is the cross-section of an individual loop, then Eq. (5) can be used to express f as a function of the known quantities, i.e.

$$f \simeq 2 \times \frac{1.44 \times 10^{-13}\alpha EM}{4\pi RT^4} \tag{13}$$

where the extra factor of 2 accounts for the fact that we only see one hemisphere of the star at any given time.

Thus for the hot component of the quiescent emission seen in the ASCA observation ($EM = 2.3 \times 10^{51}$ cm^{-3}), and assuming that quiescent loops have the same size as flaring ones ($\alpha \simeq 0.3$) one can derive $f \simeq 6\%$ (independent of β). Simple application of the scaling law (Eq. (5)) also yields estimates for the density ($n \simeq 5 \times 10^{10}$ cm^{-3}) and pressure ($P \simeq 70$ dyne cm^{-2}) of the "quiescent" loops. Our results therefore point to a corona in which the "hot" component is composed of loops with comparable relative sizes as the solar active region loops (i.e. $L \simeq 0.3\ R_*$), but with significantly higher pressure (by approximately an order of magnitude, typical solar active region loop pressures being $P_\odot \simeq 5$ dyne cm^{-2}). The required filling factor is small, i.e. only a small fraction of the stellar surface needs to be covered by such loops to explain the observed emissivity.

4.5. Metal abundance of the quiescent corona

The initial results from the ASCA observations of coronal sources, e.g. that the metal abundance of the coronal plasma is apparently "non-solar" has prompted a lively debate about the possible presence of fractionation mechanisms which would deplete the plasma along its way from the photosphere and chromosphere toward the corona. Mechanisms of this type are apparently at work in the Sun, were coronal abundance ratios are different from photospheric ones, with elements selectively enhanced on the basis of their first ionization potential (FIP). The solar corona however appears to be in general terms to be metal-enriched, rather than metal-depleted. While there is strong evidence, for example, that the coronal metal abundance changes significantly during large flares (e.g. on Algol, Stern et al. 1992; Ottmann & Schmitt 1996; Favata & Schmitt 1999), detailed assessments of the relative coronal versus photospheric abundances in stellar coronae have been hindered by the lack of detailed photospheric abundance analyses in most active stars (even on Algol it's unclear if the quiescent coronal abundance is higher or lower than the photospheric value). The situation is further complicated by the often contradictory results when such analyses are available (e.g. the contrasting results about photospheric abundances of active binaries, Randich et al. 1993 versus Ottmann et al. 1998).

In the case of AD Leo, the availability of a recent, high-dispersion spectral analysis of the photospheric Fe abundance allows a detailed comparison with the coronal abundance as derived from the X-ray observation. The photospheric metallicity of AD Leo ($[\mathrm{Fe/H}] = -0.75$, Jones et al. 1996) is at the low end of the disk population abundance range. The ASCA observation shows no evidence for differences between the coronal and photospheric Fe abundance. The coronal abundance ratios are clearly different from the solar photospheric values ($[\mathrm{Si/Fe}] \simeq [\mathrm{O/Fe}] \simeq 4$); however, while neither Si nor O abundance have been determined in the photosphere, $[\alpha/\mathrm{Fe}]$ (the abundance of elements such as Si and O, the so-called α elements) is known to be generally enhanced in low-metallicity stars, with $[\alpha/\mathrm{Fe}] \simeq 0.4$ at $[\mathrm{Fe/H}] \simeq -1.0$ (see the review of McWilliam 1997), so that even the "anomalous" abundance patterns of the AD Leo corona are in full agreement with the expected photospheric abundance ratios, and therefore no chem-

ical fractionation mechanism is required to explain the observed abundances in the quiescent corona of AD Leo.

5. Conclusions

Our results shows that the frequent flares which have been observed on the "typical" dMe star AD Leo have all taken place in similar, compact coronal loops. In all cases sustained heating is present, and the flare decay is dominated by the time evolution of the heating. As a consequence, estimates of the size of the flaring regions found assuming that the loop is decaying undisturbed will significantly overstimate the loop size, by factors (for the AD Leo flares) of $\simeq 5$.

The number of observations is such to allow to estimate the frequency of significant flares in AD Leo: adding to the *Einstein*, ROSAT and ASCA observations discussed here with the EXOSAT observations (which covered $\simeq$ 110 ks[4] and in which one flare was observed, Pallavicini et al. 1990) and with the SAX observation ($\simeq$ 40 ks exposure, three flares, Sciortino et al. 1999), a total of 10 flares have been detected on AD Leo in a total of 480 ks, yielding an average flaring rate of one flare every approximately 50 ks (which does not include the several minor flaring events visibile both in the PSPC and in the SIS light-curves).

The small range of sizes for the flaring loops (on the assumption that the same class of loops is also the main component of the active corona) implies a corona which scales to larger luminosities by filling relatively compact loop structures (similar to the solar ones) with progressively higher pressure plasma. A pressure about 10 times the typical value for solar active regions is sufficient, with a small filling factor $f \simeq 6\%$. Such a scenario is well in agreement with the compact high-pressure loops with $f \ll 1$ which both Giampapa et al. (1996) and Sciortino et al. (1999) derive for AD Leo as well as other flare stars through the spectral analysis of the quiescent coronal emission.

These conclusions are somewhat difficult to reconcile with the scenario discussed by Drake et al. (1999), in which the intermediate activity levels are reached by increasing the filling factor of solar-like (in size and pressure) active regions up to $f \simeq 1$. The approximate filling factor we derive is $f \ll 1$, and the large emissivity is fully explained by the increase in pressure. The flare emission can be explained through a significant (about two order of magnitudes over the quiescent value) increase in pressure in the same loops responsible for the quiescent emission. However Drake et al. (1999) based their conclusions on the observation of solar-type stars, where in principle the scaling mechanism to high X-ray luminosity could be different from the one in flare stars.

The discrepancy between the pressure derived for the flaring loops through the application of the Rosner et al. (1978) scaling laws and the pressure determined from the peak emission measure and temperature assuming loops with a solar-like aspect ratio ($\beta \simeq 0.1$) points at the stellar loops having larger volumes for a given length than in the solar case, which can be obtained with a larger β, i.e. with "fatter" loops. A value of $\beta \simeq 0.3$ is sufficient to reconcile the two estimates of pressure.

The upcoming high spectral resolution observations of the X-ray emission from both the quiescent and flaring emission from flare stars, to be performed with the *Chandra* and XMM observatories will allow direct measurements of the plasma pressure for a range of temperatures using selected spectral diagnostics, and thus to test the correctness of the framework presented in the present paper. Although high-resolution spectroscopy will certainly be a more powerful method for the study of the coronal structuring of active stars than the study of flare decay, the approach used here will still be important in the *Chandra*-XMM era as it will be applicable to a much larger number of stars (hence spanning a broad range of stellar parameters) than high-resolution spectroscopy. Also, the pressures derived through high-resolution spectroscopy will be weighted by the plasma emissivity and thus, if significant filamentation within loops is present, can in principle be much higher than the average pressure implied by the loop's length and emission measure; such evidence has been reported in the solar case (e.g. Phillips et al. 1996). Therefore, comparison of the spectroscopically measured pressures with the flare-derived emission-measures and lengths will constitute a valuable diagnostic of structuring within a single coronal loop.

The quiescent X-ray luminosity of AD Leo is remarkably constant across almost 20 yr, i.e. between the *Einstein* IPC observation in 1980 and the 1997 SAX observation it ranges from $\simeq 3 \times 10^{28}$ erg s^{-1} (in 1980) and $\simeq 5 \times 10^{28}$ erg s^{-1} (in 1996), a remarkably small range also given the diversity of the various instruments used in the comparison. As recently reviewed by Stern (1998), active stars show no evidence of a cyclic behavior in their activity level, and indeed AD Leo is no exception.

Acknowledgements. G. Micela and F. Reale acknowledge the partial support of ASI and MURST. This research has made use of data obtained through the High Energy Astrophysics Science Archive Research Center (HEASARC) Online Service, provided by the NASA/Goddard Space Flight Center.

Appendix A: Physical characteristics of AD Leo and other X-ray observations

AD Leo (Gl 388) is classified as dM3e (Henry et al. 1994), and its distance (from the ground-based parallax, Gray & Johanson 1991 – AD Leo wasn't a Hipparcos target) is 4.9 pc. No companions to it are known (Reid & Gizis 1997). It is one of the few M dwarfs for which a high resolution abundance analysis of its photospheric spectrum is available: using state of the art model atmospheres and near-IR high-resolution spectra Jones et al. (1996) have estimated the photospheric parameters at $T_{\rm eff} = 3350$, [Z/H] $= -0.75 \pm 0.25$ and $\log g = 4.5$. Its measured rotational velocity ($v \sin i = 6.2 \pm 0.8$ km s^{-1}) places AD Leo among the tail of rare, fast rotating M

[4] The EXOSAT high orbit resulted in continuous time coverage, unlikely the other low-Earth orbit satellites, which have a $\simeq 50\%$ duty cycle, and thus the two data sets are not fully homogeneous, and the resulting flaring rate is only approximate.

dwarfs (Delfosse et al. 1998); the photometrically-determined rotational period is 2.7 d (Spiesman & Hawley 1986).

The bolometric luminosity of AD Leo (Delfosse et al. 1998) is $M_{\rm bol} = 8.85$ (corresponding to a bolometric luminosity $L_{\rm bol} = 8.7 \times 10^{31}$ erg s^{-1}). The K-band absolute luminosity is $M_K = 6.26$ (from the average apparent K-band magnitude reported by Leggett 1992, and using $d = 4.9$ pc), which, through the mass-luminosity relationship of Baraffe et al. (1998), yields $M = 0.40\ M_\odot$. Using the models of Chabrier & Baraffe (1997), the radius at $M = 0.40\ M_\odot$ is 2.64×10^{10} cm at $[{\rm M/H}] = 0$, and 2.57×10^{10} cm at $[{\rm M/H}] = -1$. Based on the above-mentioned abundance determination we have assumed $R = 2.6 \times 10^{10}$ cm ($\simeq 0.37\ R_\odot$). At this mass (Chabrier & Baraffe 1997), stars are expected to have a substantial radiative core, so that the interior structure is still "solar-like".

A.1. Other X-ray observations

The first X-ray flare on AD Leo was seen with the HEAO 1 A-2 soft X-ray detector (Kanh et al. 1979; who also show that the identification of AD Leo with a quiescent HEAO 1 source by Ayres et al. 1979 was not correct). The approximate flaring X-ray luminosity reported is $\simeq 10^{30}$ erg s^{-1}, with a peak emission measure of $\simeq 10^{53}$ cm^{-3}.

The *Einstein* observation is discussed in Sect. 2.1, while EXOSAT observed AD Leo in four different occasions (Pallavicini et al. 1990), either as a pointed target or serendipitously, for a total of $\simeq 110$ ks. The quiescent X-ray luminosity reported was 5×10^{28} erg s^{-1}, and one flare was observed, with a rise time ($1/e$) of 10 min and a decay time of 60 min. The flare represented a factor of 12 enhancement over the quiescent flux, with peak X-ray luminosity $L_{\rm X} = 4.2 \times 10^{29}$ erg s^{-1} and a total energy release estimated at 1.5×10^{33} erg.

ROSAT observed AD Leo with the PSPC detector on May 8, 1991. The resulting average spectrum was analyzed by Giampapa et al. (1996) – who used the Raymond & Smith (1977) plasma emission code – and later reanalyzed by Sciortino et al. (1999) using the MEKAL plasma emission code. The average PSPC spectrum (including the two flaring events) analyzed with the MEKAL code is compatible with a two-temperature model with metallicity $Z = 0.1\ Z_\odot$, best-fit temperatures of 6.6 and 16 MK, and emission measures of 16×10^{51} cm^{-3} and 2.7×10^{51} cm^{-3}, respectively. The average (including flares) X-ray luminosity is $L_{\rm X} = 9 \times 10^{28}$ erg s^{-1}. To fit the spectrum a larger interstellar column density than compatible with the EUV observations is required ($N({\rm H}) = 1.7 \times 10^{19}$ cm^{-2}), similarly to many other coronal sources.

AD Leo was also the target of a day-long SAX observation on April 23, 1997, discussed by Sciortino et al. (1999). Continuous variability is evident in the light curve, with at least three recognizable individual flaring events with enhancements over the "quiescent" count rate of $\simeq 5$ times (in the 1.5–7.0 keV band) and decay times of $\simeq 0.8$, 4.0 and 4.4 ks, with insufficient counts for a detailed analysis. The total spectrum (including the flaring events) needs three thermal components to be well fit, with the first two components at temperatures of 3.7 and 12 MK, and a third (effectively unbound) component at $T \gtrsim 100$ MK. The average X-ray luminosity in the 0.1–7.0 keV band is 4×10^{28} erg s^{-1}. The SAX spectrum can also be fit with static loop models, resulting in two classes of loops, one with $T_{\rm max} = 13$ MK and the second with $T_{\rm max} \gtrsim 100$ MK. The cooler loops are compact ($L \lesssim 0.1\ R_*$) and with a small filling factor ($f \lesssim 10^{-3}$), while the size and filling factor of the hotter loops are not constrained by the fit.

Finally, a long EUVE observation of AD Leo was performed in March 1993, during which two flaring events where seen, which have been analyzed by Cully et al. (1997). Their analysis is discussed in detail in Sect. 4.

Table B.1. The coefficients (mean values, standard deviations and weights) for the computation of the *Einstein* IPC spectral shape index using Eqs. (3) and (4) of Reale & Micela (1998). The usage of PI channels is assumed.

C	$\langle C \rangle$	σ_C	W	C	$\langle C \rangle$	σ_C	W
1	.1646	.0634	0.36	6	.0825	.0301	−0.36
2	.1931	.0548	0.36	7	.0559	.0272	−0.36
3	.1731	.0228	0.33	8	.0360	.0224	−0.35
4	.1456	.0178	−0.18	9	.0222	.0169	−0.33
5	.1139	.0280	−0.33				

Appendix B: Derivation of flare parameters for the Einstein IPC

Although less sensitive, the *Einstein* IPC detector is in many respects similar to the ROSAT PSPC. The main difference is the lower spectral resolution, with the incoming photon energy being coded in only 15 energy channels. The approach taken for the analysis of flares seen in IPC data closely mirrors the one used for the analysis of PSPC data, described in detail in Reale & Micela (1998). Here we will only describe the IPC-specific differences, and refer the reader to Reale & Micela (1998) for a detailed description.

The essential difference between the approach used for the ASCA SIS data (for which spectral temperatures are derived from a fit to isothermal models) and the one used for the PSPC and for the IPC is the definition, for the latter two detectors, of a temperature indicator based on a linear combination of the photon counts in each detector channel. This "spectral-shape index" (SSI) is obtained through a principal-component analysis, and is, for low-resolution detectors, more robust than a fit to the spectrum. Similarly, the square root of the count rate (CR2) is used as a proxy to the density, so that the $\log n$–$\log T$ diagram (e.g. Fig. 7) is replaced by a "CR2–SSI" diagram.

In the case of the IPC the spectral-shape index has been obtained taking the first 10 PI channels, of which the first 9 are considered as the independent ones. The values of the $\langle C_i \rangle$ and σ_{C_i} coefficients and the weights to calculate the spectral-shape index for the IPC (using Eqs. (3) and (4) of Reale & Micela 1998) are listed in Table B.1. The relationship linking the ratio of the

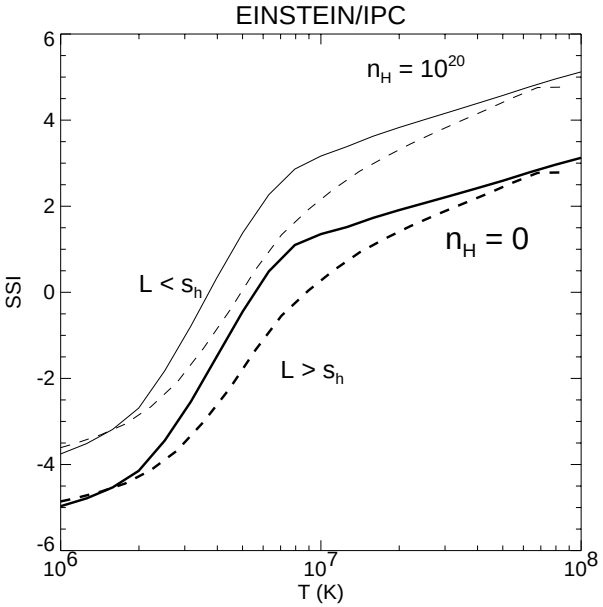

Fig. B.1. The Spectral Shape Index (SSI) of *Einstein* IPC spectra as a function of the maximum temperature of hydrostatic loop models (cf. Fig. 1 of Reale & Micela 1998) with length much shorter (*solid lines*) and longer (*dashed lines*) than the local pressure scale height (s_h).

observed decay time $\tau_{\rm LC}$ and the intrinsic thermodynamic decay time $\tau_{\rm th}$ with the slope ζ determined in this case in the CR2–SSI diagram (the equivalent of Eq. (4)) is

$$\tau_{\rm LC}/\tau_{\rm th} = c_I e^{(\zeta/\zeta_I)} + q_I = F_I(\zeta) \qquad \text{(B.1)}$$

with:

$$c_I = 5.91 \qquad \zeta_I = -0.34 \qquad q_I = 1.74$$

For large flaring loops (i.e. loops larger than the local pressure scale height) the relationship is:

$$\tau_{\rm LC}/\tau_{\rm th} = c'_I e^{(\zeta/\zeta'_I)} + q'_I = F'_I(\zeta) \qquad \text{(B.2)}$$

with

$$c'_I = 76.9 \qquad \zeta'_I = -1.30 \qquad q'_I = 1.52$$

Fig. B.1 shows the dependence of the IPC SSI on the temperature at the top of model hydrostatic loops, analogous to Fig. 1 of Reale & Micela (1998), to be applied to infer the flare maximum temperature, which is to be used in Eq. (4) for deriving the loop length.

The distribution of predicted vs. true model loop lengths is well centered around the correct value (median + 2%) with a standard deviation of 18%. Simulations analogous to those described in Sect. 2.4 of Reale & Micela (1998) show that an uncertainty between 10% and 30% (for 10 000 cts per bin) must be added, depending on the heating time scale $\tau_{\rm H}$ (going from $\tau_{\rm H} = 0$ to $\tau_{\rm H} = 2\tau_{\rm th}$). For 1000 cts per bin the uncertainties are much larger than with PSPC ($> 80\%$), likely because the lower spectral resolution induces a large indetermination in the slope in the CR2–SSI diagram.

References

Ambruster C.W., Sciortino S., Golub L., 1987, ApJS 65, 273
Ayres T.R., Linsky J.L., Garmire G., Cordova F., 1979, ApJ 232, L117
Baraffe I., Chabrier G., Allard F., Hauschildt P.H., 1998, A&A 337, 403
Brickhouse N.S., Dupree A.K., 1998, ApJ 502, 918
Chabrier G., Baraffe I., 1997, A&A 327, 1039
Cully S.L., Fisher G.H., Hawley S.L., Simon T., 1997, ApJ 491, 910
Delfosse X., Forveille T., Perrier C., Mayor M., 1998, A&A 331, 581
Drake J.J., Peres G., Orlando S., Laming J.M., Maggio A., 1999, ApJ submitted
Favata F., Schmitt J.H.M.M., 1999, A&A 350, 900
Favata F., Reale F., Micela G., et al., 2000, A&A in press
Fisher G.H., Hawley S.L., 1990, ApJ 357, 243
Giampapa M.S., Rosner R., Kashyap V., et al., 1996, ApJ 463, 707
Gray D.F., Johanson H.L., 1991, PASP 103, 439
Hawley S.L., Fisher G.H., Simon T., et al., 1995, ApJ 453, 464
Henry T.J., Kirkpatrick J.D., Simons D.A., 1994, A&A 108, 1437
Johns-Krull C.M., Valenti J.A., 1996, ApJ 459, L95
Jones H.R.A., Longmore A.J., Allard F., Hauschildt P.H., 1996, MNRAS 280, 77
Kanh S.M., Linsky J.L., Mason K.O., et al., 1979, ApJ 234, L107
Leggett S.K., 1992, ApJS 82, 351
McWilliam A., 1997, ARA&A 35, 503
Mewe R., 1992, in R. Pallavicini (ed.), Solar and stellar coronae, Vol. 63 of *Mem. Soc. Astron. Ital.*, SAIt, p. 681
Mewe R., Kaastra J.S., Liedahl D.A., 1995, Legacy 6, 16
Morrison R., McCammon D., 1983, ApJ 270, 119
Orlando S., Peres G., Reale R., Rosner R., Hudson H., 2000, in R. Pallavicini (ed.), Star clusters and associations, ASP Conference Series, ASP, San Francisco, in press
Ottmann R., Schmitt J.H.M.M., 1996, A&A 307, 813
Ottmann R., Pfeiffer M.J., Gehren T., 1998, A&A 338, 661
Pallavicini R., Tagliaferri G., Stella L., 1990, A&A 228, 403
Peres G., Orlando S., Reale F., Rosner R., Hudson H., 2000, ApJ in press
Phillips K.J.H., Bhatia A.K., Mason H.E., Zarro D.M., 1996, ApJ 466, 549
Randich S., Gratton R.G., Pallavicini R., 1993, A&A 273, 194
Raymond J., Smith B., 1977, ApJS 35, 419
Reale F., Micela G., 1998, A&A 334, 1028
Reale F., Betta R., Peres G., Serio S., McTiernan J., 1997, A&A 325, 782
Reid N.I., Gizis J.E., 1997, AJ 113, 2246
Rosner R., Tucker W.H., Vaiana G.S., 1978, ApJ 220, 643
Schmitt J.H.M.M., 1998, in R. A. Donahue, J.A. Bookbinder (eds.), Cool Stars, Stellar Systems and the Sun, Vol. 154 of *ASP Conference Series*, ASP, San Francisco, 463
Schmitt J.H.M.M., Favata F., 1999, Nat 401, 44
Schmitt J.H.M.M., Collura A., Sciortino S. et al., 1990, ApJ 365, 704
Schmitt J.H.M.M., Drake J.J., Stern R.A., Haisch B.M., 1996a, ApJ 457, 882
Schmitt J.H.M.M., Drake J.J., Haisch B.M., Stern R.A., 1996b, ApJ 467, 841
Sciortino S., Maggio A., Favata F., Orlando S., 1999, A&A 342, 502
Serio S., Reale F., Jakimiec J., Sylwester B., Sylwester J., 1991, A&A 241, 197
Spiesman W.J., Hawley S.L., 1986, AJ 92, 664
Stern R., 1998, in R.A. Donahue, J.A. Bookbinder (eds.), Cool Stars, Stellar Systems and the Sun, Vol. 154 of *ASP Conference Series*,

ASP, San Francisco, 223
Stern R.A., Uchida Y., Tsuneta S., Nagase F., 1992, ApJ 400, 321
Sylwester B., Sylwester J., Serio S. et al., 1993, A&A 267, 586
van den Oord G.H.J., Mewe R., 1989, A&A 213, 245
Ventura P., Zeppieri A., Mazzitelli I., D'Antona F., 1998a, A&A 331, 1011
Ventura R., Maggio A., Peres G., 1998b, A&A 334, 188